# Object-Based Cognitive Map in the Human Hippocampus and Medial Prefrontal Cortex

**Authors: Bo Zhang[1] and Yuji Naya[1, 2, 3, 4, 5, *]**

**Affiliations:**

[1] School of Psychological and Cognitive Sciences, Peking University, No. 52, Haidian Road, Haidian District, Beijing 100805, China

[2] Center for Life Sciences, Peking University, No. 52, Haidian Road, Haidian District, Beijing 100805, China

[3] IDG/McGovern Institute for Brain Research at Peking University, No. 52, Haidian Road, Haidian District, Beijing 100805, China

[4] Beijing Key Laboratory of Behavior and Mental Health, Peking University, No. 52, Haidian Road, Haidian District, Beijing 100805, China

[5] Lead contact

**Contact Info:** *Correspondence: yujin@pku.edu.cn

**Summary**

A cognitive map, representing an environment around oneself, is necessary for spatial navigation. However, compared with its constituent elements such as individual landmarks, neural substrates of coherent spatial information remain largely unknown. The present study investigated how the brain codes map-like representations in a virtual environment specified by the relative positions of three objects. Representational similarity analysis revealed an object-based spatial representation in the hippocampus (HPC) when participants located themselves within the environment, while the medial prefrontal cortex (mPFC) represented it when they recollected a target object's location relative to their self-body. During recollection, task-dependent functional connectivity increased between the two areas implying exchange of self- and target-location signals between HPC and mPFC. Together, the coherent cognitive map, which could be formed by objects, may be recruited in HPC and mPFC for complementary functions during navigation, which may generalize to other aspects of cognition, such as navigating social interactions.

**Key words:** cognitive map, spatial navigation, episodic memory, memory-guided decision making, social interaction, hippocampus, medial prefrontal cortex, default-mode network, representational similarity analysis.

## Introduction

During navigation, it is necessary to locate our self-position in the current spatial environment as well as to locate the objects relative to the self-body (i.e., egocentric location). To conduct each of the two mental operations, we need map-like representations, called "cognitive map" in our brain (Tolman, 1948). After the discovery of "place cells," the hippocampus (HPC) of the medial temporal lobe (MTL) has been considered responsible for the cognitive map (Buffalo, 2015), and crucial contributions of the HPC to spatial memory have also been reported by animal model studies that evaluated behavioral patterns of rodents with an inactivated HPC using the Morris water maze and cross-maze (Nakazawa et al., 2002; Packard and McGaugh, 1996; Redish and Touretzky, 1998) as well as human studies that demonstrated the relationship between HPC volume in individual subjects and their amounts of experience exploring spatial environments (Woollett and Maguire, 2011; Schinazi et al., 2013, e.g., London taxi drivers). However, it remains largely unknown how neural substrates of the cognitive map are involved in the two mental operations required to locate specific objects within the environment. One possible reason for the difficulty in addressing this question is that despite extensive studies on the spatial elements related to the cognitive map (e.g., self-location, head-direction etc.) (O'Keefe and Dostrovsky, 1971; Vass and Epstein, 2013; Chadwick et al., 2015; Buffalo, 2015; McCormick et al., 2018;), there is still a lack of sufficient isolation and characterization of the neural signal of the cognitive map under the previous research paradigms.

In addition to the HPC, the role of the medial prefrontal cortex (mPFC) in goal-directed planning during navigation was demonstrated by a previous human fMRI study that showed increased connectivity between the HPC and mPFC (Brown et al., 2016). The mPFC has been long considered as a member of the core-brain system in the retrieval of episodic memory (Konishi et al., 2000; Eichenbaum, 2017; McCormick et al., 2018), which is an

62 autobiographical memory consisting of spatial, object, and temporal information (Suzuki and
63 Naya, 2011; Naya and Suzuki, 2011; Squire and Wixted, 2011). Schacter et al. (2007)
64 suggested an involvement of the mPFC in future-simulation processing and recollection of
65 past episodes, which depend on mnemonic information stored as declarative memory
66 including both episodic and semantic memory. Recently, they also showed increased
67 connectivity between the HPC and mPFC during future simulation (Campbell et al., 2018).
68 This preceding literature suggests that the HPC and mPFC, which belong to the default-mode
69 network, work together when remembering stored information (e.g., cognitive map) and
70 construct the mental representation of goal-directed information (e.g., target-location) from
71 mnemonic information with the current context (e.g., self-location) (Schacter, 2012).
72 However, the specific functional role of each of HPC and mPFC during the construction
73 process (McCormick et al., 2018; Campbell et al., 2018) remain elusive, presumably because
74 the construction of goal-directed information (e.g., spatial navigation) includes at least two
75 mental operations described above (locating the self and locating an object target relative to
76 self-location), as previous experimental paradigms did not dissociate these aspects of
77 behavior.

78 To address these issues, we aimed to devise a novel 3D spatial-memory task with
79 spatial environments defined by objects, which would enable us to identify the representation
80 of the cognitive map and to investigate how it is related to the two mental operations (Fig. 1).
81 We used a stimulus set consisting of three different human characters throughout the entire
82 experiment, while the spatial configuration of the three characters was changed in a trial-by-
83 trial manner. The spatial configuration pattern was referred to as a *"map"* in the present
84 study (Fig. 1b). In each trial, participants encoded a *map* from the first-person's view by
85 walking toward the characters in one of four fixed walking directions (walking period, Fig.
86 1c, see Methods). Following the walking period, one human character (facing object) was

presented on a virtual-environment background with other characters being invisible, which gave the participants a feeling of facing the presented character in the virtual environment (i.e., facing period). After a short delay, one of the two remaining characters (targeting object) was presented without the virtual environment background, and the participants were required to remember the location of this second human character relative to their self-body (i.e., targeting period). Thus, the two mental operations were separated into two periods within a single trial. This task design allowed us to detect the brain regions that distinguished the spatial configurations of the objects (i.e., *map*) around the participants during the facing period and targeting period separately. The results of the representational similarity analysis (RSA; see Methods for details) (Kriegeskorte et al., 2012; Kriegeskorte et al., 2008) showed that the spatial environment defined by the three objects were represented in the HPC during the facing period, while it was represented in the mPFC during the targeting period, suggesting different contributions of the object-based cognitive map to the recollection between the two brain areas of the default-mode network.

## Results

The experiment was conducted over two days with 19 participants. On the first day, the participants were familiarized with the 3D virtual environment and the three human characters through a head-nodding detection (HND) task (Fig. S1a). In this task, the participants had the same walking experience as in the spatial-memory task but were subsequently asked to indicate whether one of the three characters in a photo had nodded its head during the walking period. On the second day, the participants performed the spatial-memory task during fMRI scanning (Fig. 1a). To prevent voluntary memorization of the spatial relationship of the human characters during the walking period, the HND trials were pseudo-randomly mixed with the spatial-memory trials at the ratio of 1:10, and the participants were instructed to focus on head-nodding of the human characters during the walking period in all trials. In each trial, its trial-type (i.e., HND or memory task) became distinguishable after the walking period by subsequent stimuli. All participants exhibited ceiling performance with a 93.6% ± 0.02% correct rate (mean ± SE, n = 19) for the spatial-memory task and no significant difference was found among each of the task parameters (e.g., maps, walking directions) (Fig. S1c). All participants also showed accuracy that was significantly higher than chance level (50%) in both the head-nodding and no head-nodding trials in the HND task (Fig. S1a). Attempts to memorize the spatial arrangements of the human characters during scanning were examined using post-scanning questionnaires. All participants reported that they did not make any voluntary effort to memorize the spatial relationship of the three human characters nor utilize any special strategy for memorizing it (Table S2). It should be noted that no participant was able to recall the number of map patterns they experienced in the experiment even though only three of the six possible patterns of maps were repeatedly presented to each participant. In addition, no significant changes in performance was found across four experimental sessions (Fig. S1b; $F(3,72) =$

126 0.38, P = 0.76), suggesting that the participants performed the spatial-memory task with high-
127 performance from the beginning and did not learn to use a systematic strategy to improve
128 their performance during the sessions. These behavioral results guarantee that the participants
129 automatically encoded maps during the walking period when viewing the human characters
130 attentively to detect head-nodding.
131
132 **Neural representation of the cognitive map during locating self-position**
133 We first assessed the map representation during the facing period (4.0 s including the
134 subsequent delay; Fig. 2a), in which the participants oriented themselves to a presented
135 human character in the 3D environment. To decode the map information across the whole
136 brain, we conducted searchlight-based RSA, which compared the multi-voxel pattern
137 similarities of the "same map" and "different map" between trial pairs across each brain
138 voxel by drawing a 6 mm radius sphere with each voxel in the spherical center. Map
139 information was decoded regardless of other task parameters such as the walking direction or
140 the identity of the facing character by balancing the number of trials with other task
141 parameters across the same and different map conditions during the scanning as well as
142 excluding the effects of other task parameters in the regression analysis (see Methods for
143 details and Table S1 for the regressor list and the averaged $r^2$ among the regressors in each
144 GLM). We found a cluster located in the left middle HPC (mHPC; Fig. 2b, $P < 0.01$, voxel-
145 wise threshold; $P < 0.05$, cluster-corrected for multiple comparison), suggesting that the map
146 defined by multiple objects is represented in the HPC. In addition to the mHPC, the
147 searchlight-based RSA revealed clusters in the insula, angular gyrus, and superior temporal
148 cortex (Fig. S2b, $P < 0.01$, voxel-wise threshold; $P < 0.05$, cluster-corrected for multiple
149 comparison; see discussion). To validate the searchlight-based RSA result showing that the
150 left mHPC represents map information, we manually segmented the sub-regions in the MTL

151 in each participant's native space (Fig. S4a, top panel) and conducted an independent RSA
152 within each anatomical mask (see Methods for details). The region of interest (ROI)-based
153 result also showed that only the left mHPC had a significantly higher pattern similarity to
154 "same maps" relative to "different maps" among the MTL sub-regions (Fig. S5a; $t(18) =$
155 $3.26$, $P = 0.002$, Bonferroni corrected for multiple comparisons, alpha $< 0.05$).

156 To examine possible signal input from the MTL sub-regions to the left mHPC for the
157 map construction, we examined the neural representation of the facing-character identity and
158 walking direction that the participants perceptually and/or mentally re-experienced during the
159 facing period based on the post-scanning test (Table S2; Fig. S3a). Searchlight-based RSA
160 revealed that the bilateral perirhinal cortex (PRC) encoded character identity (Fig. S3b; $P <$
161 $0.001$, initial threshold; $P < 0.05$, cluster-corrected for multiple comparison) (Naya et al.,
162 2001; Suzuki and Naya, 2014), while the parahippocampal cortex (PHC) and left
163 retrosplenial cortex (RSC) encoded the walking directions reflecting the spatial layout of one
164 empty and three occupied positions perceived by the participants during the walking period
165 (Fig. 1c). In the HPC, the left posterior HPC (pHPC) selectively represented the spatial layout
166 but not the character identity, while the bilateral anterior HPC (aHPC) revealed clusters for
167 both character identity and spatial layout (Fig. S3b). These results were consistent with the
168 notion of the "two cortical systems" model suggesting that object identity and spatiotemporal
169 context are processed in two separate neural systems with the PRC and PHC-RSC as the core
170 brain regions, with the two different information domains interacting in the HPC (Ranganath
171 and Ritchey., 2012). Together, the RSA analyses suggest that the MTL is associated with
172 representing the spatial environment in the following ways**:** elements such as each object
173 identity and spatial layout are represented by extrahippocampal areas while the relative
174 relationship between multi-objects is represented in the HPC, suggesting cognitive map
175 representation in the HPC.

**Cognitive map during localizing target**

In contrast to locate self-position, a clear difference was found in brain regions responsible for the map representations when the participants remembered the location of a target character relative to their self-body (egocentric target location). In contrast to the facing period, clusters representing the map information were revealed mainly in the Rectus and Brodmann area 10 of the mPFC (Peak coordinates: 4, 50, -18; t value: 5.62), rather than in the HPC, during the targeting period. We confirmed that no cluster was found in the MTL even though a more liberal threshold was used ($P < 0.01$, voxel-wise threshold, uncorrected). To validate this result, we conducted an independent RSA using frontal sub-regions of the automated anatomical labeling (AAL, Fig. S4a, bottom panel) template as well as manually segmented MTL sub-regions as ROIs. The result confirmed that the map information was represented in the rectus of the prefrontal region (Fig. S5a, left: $t(18) = 3.67$, $P = 0.0008$, right: $t(18) = 4.49$, $P = 0.0001$, Bonferroni corrected for multiple comparisons, alpha < 0.05), while no MTL sub-regions including the left mHPC revealed map representation significantly during the targeting period. Together with the facing period results, these results revealed a double dissociation of the HPC and mPFC function in the map representation between the task demands, implying that the mPFC, rather than the HPC, carried the map information during the generation of the egocentric location signal of a target character. Our results indicate that the HPC and mPFC may operate in a complementary manner, supporting the notion of the "parallel, but interactive cognitive map" between the two brain structures (Wikenheiser and Schoenbaum., 2016). Outside of the mPFC, we found clusters in the precuneus and middle temporal gyrus, and the inferior frontal cortex (Fig. 2c, Fig. S2c; $P < 0.001$, voxel-wise threshold; $P < 0.05$, cluster-corrected for multiple comparison). These three brain regions have been consistently reported to be involved in scene construction

201 during recalling of past experience and imagination of new experiences (Hassabis and
202 Maguire, 2007; Bird et al., 2010; Gaesser et al., 2013), which is consistent with the post-
203 scanning report showing that all participants recalled and also imagined the egocentric
204 positions of the three human characters during the targeting period.
205 As with the facing period, we examined neural representation of targeting character
206 identity and walking direction during the targeting period and found that the PRC stably
207 represented character identity (Fig. S3b; $P < 0.001$, initial threshold; $P < 0.05$, cluster-
208 corrected for multiple comparison), while we did not find clusters for the spatial layout
209 depending on the walking direction in the MTL. These results suggested that the HPC did not
210 construct the map information from its constituent elements during the targeting period.
211
212 **Current self-orientation on the map**
213 To compute the egocentric location of a target object (e.g., left, right, or back), information
214 on the current self-position/orientation on the map is necessary (Fig. 3a). Therefore, we
215 examined which brain regions were involved in representing such allocentric "heading-
216 direction" signals (Hargreaves et al., 2005; Wang et al., 2018). Interestingly, while no
217 significant cluster was revealed during the facing period (facing character; Fig. 3b and
218 Supplementary Fig. S5b), robust clusters were revealed during the targeting period (Fig. 3b, P
219 $< 0.001$, voxel-wise threshold; $P < 0.05$, cluster-corrected for multiple comparison). These
220 clusters were located in the left ERC, bilateral HPC and PHC inside the MTL as well as in
221 the lateral occipital cortex, parietal cortex, precuneus, and anterior cingulate cortex outside
222 the MTL (Fig. 3b, $P < 0.001$, voxel-wise threshold; $P < 0.05$, cluster-corrected for multiple
223 comparison). These results suggested that a self-orientation signal was induced during the
224 targeting period, presumably because of the necessity to compute the egocentric target

225 location. This interpretation is consistent with the post-scanning report in which participants
226 reported imagining their self-orientation on the map only during the targeting period.
227
228 **Remembering the egocentric location of a target object**
229 Next, we examined which brain regions signaled the egocentric location (left, right, or back
230 relative to self-body) of a target object (Fig. 4a). The results revealed robust clusters in both
231 the mPFC and MTL (Fig. 4a, $P < 0.001$, voxel-wise threshold; $P < 0.05$, cluster-corrected for
232 multiple comparison). In the mPFC, we identified the rectus, medial/superior orbitofrontal
233 cortex, and olfactory cortex. In the MTL, clusters were found in the anterior HPC. Apart from
234 the mPFC and MTL, clusters were also found in the lateral occipital cortex, inferior parietal
235 cortex, anterior temporal lobe, premotor cortex, and lPFC (middle and superior PFC). We
236 also found clusters in the precuneus and posterior parietal cortex, which were previously
237 reported to represent the egocentric location (Chadwick et al., 2015). The widely distributed
238 clusters may indicate that the brain regions representing the egocentric target locations can be
239 involved in either generation of the egocentric-target-location information from multiple
240 pieces of information (cognitive map, self-orientation, and target character identity) or its
241 maintenance while preparing for the following response. These distinct functions might be
242 supported by three different large-scale brain networks: the dorsal attention network,
243 frontoparietal control network, and default-mode network (Spreng and Schacter., 2011). In
244 contrast to the robust signal observed across different brain networks for egocentric target-
245 location, no cluster was revealed for allocentric target location relative to the spatial layout of
246 the characters (Fig. 4b, $P < 0.001$, voxel-wise threshold; $P < 0.05$, cluster-corrected for
247 multiple comparison), which implies that the target location may be directly retrieved in the
248 form of egocentric coordinates rather than via its allocentric representation.
249

**Increased default-mode network connectivity while locating a target compared with self-locating**

The present results showed that the MTL and mPFC signaled a coherent map coding a spatial relationship of the three human characters during the different time periods in which different task demands were required (i.e., self-locating and target-locating). In addition, the MTL and mPFC signaled the different location information even during the same targeting period; MTL areas tended to represent allocentric self-location while the mPFC tended to represent egocentric target location. To investigate how the different functional contributions of the MTL and mPFC were substantiated by whole brain large-scale networks, we conducted a task-based functional connectivity analysis using MTL and mPFC sub-regions as seeds (six and four, respectively). For each seed, the mean regional bold signals associated with two TRs in each of facing and targeting period were estimated in each trial, and concatenated across trials to make its task-based time course, which contains 72 time points (i.e., 2 TRs × 36 trials) in each session. The task-based time course of the regional signal for each seed was correlated with each voxel's time course outside the seed and then was averaged across the four sessions for each participant, generating seed-based connectivity maps for each of facing and targeting periods (Ranganath et al., 2005). Then, we compared the connectivity between the two periods across the participants using a permutation test (see Methods for details).

First, we examined the connectivity between the MTL and mPFC subregions for each of task demands, the result indicated a significantly larger connectivity between the medial orbital frontal cortex and the MTL subregions in the targeting period relative to the facing period. (aHPC: $t(18)=4.75$, $P<0.001$, pHPC: $t(18)=3.96$, $P<0.001$, PHC: $t(18)=6.85$, $P<0.001$, Bonferroni corrected for multiple comparison, alpha<0.05). In addition, both the MTL and mPFC showed significantly larger connectivity to other brain areas that belong to the default-mode network and those to the dorsal attention network during the targeting period compared

275 to the facing period (Fig. 5b, $P < 0.01$, voxel-wise threshold; $P < 0.05$, cluster-corrected for
276 multiple comparison). By contrast, both the MTL and mPFC showed significantly larger
277 connectivity to the frontoparietal control network during the facing period relative to the
278 targeting period (Fig. 5a, $P < 0.001$, voxel-wise threshold; $P < 0.05$, cluster-corrected for
279 multiple comparison). These results suggest that both the MTL and mPFC changed their
280 connectivity to the three functional networks across the two task periods. We next evaluated
281 the task-based functional connectivity during each task period based on the three functional
282 network masks (Fig. S4b, Fig. 5a, b, and see method for details). This ROI analysis revealed
283 that the default-mode network was positively correlated with the MTL ($t(18) = 7.98$ for
284 average across the sub-regions within MTL, $P < 0.001$) and mPFC ($t(18) = 9.63$ for average
285 across the sub-regions within mPFC, $P < 0.001$) for both time periods with a significant
286 increase during the targeting period (Fig. 5c & Fig. S6, top panel; $F(1,72) = 4.51$, $P = 0.03$),
287 regardless of the seeds (MTL or mPFC; $F(1,72) = 0.00$, $P=0.98$). These results suggest that
288 the default-mode network contributes more to the retrieval of the target location than the self-
289 location to an external reference during the facing period. In contrast, the frontoparietal
290 control network showed significantly negative connectivity with the MTL ($t(18) = -10.50$, $P$
291 $< 0.001$) and mPFC ($t(18) = -6.55$, $P < 0.001$) during both task periods, indicating that the
292 frontoparietal control network works competitively with MTL and mPFC areas of the
293 default-mode network. This competitive effect was stronger during the targeting period (Fig.
294 5c $F(1,72) = 5.58$, $P = 0.02$, also see Fig. S6, middle panel;). Interestingly, despite both the
295 MTL and mPFC being part of the default-mode network, they showed opposite connectivity
296 patterns to the dorsal attention network during both periods (Fig. 5c & Fig. S6, bottom panel;
297 $F(1,72) = 55.07$, $P < 0.001$); the MTL positively with the network while the mPFC negatively
298 correlated with it. The connectivity between the MTL and the dorsal attention network
299 increased from the facing to targeting period ($F(1,72) = 8.43$, $P = 0.005$). These results

suggested that the dorsal attention network, which contains the superior parietal lobule (SPL) that represented egocentric target location (Fig. 4a), showed increased coupling with the MTL during the targeting period. On the other hand, the mPFC only attenuated its amplitude of anti-correlated connectivity with the dorsal attention network, which may suggest that egocentric target location represented in the mPFC was not directly transmitted to the dorsal attention network. Considering the increased coupling between the mPFC and default-mode network including MTL areas during the targeting period (Fig. 5b&c), we hypothesize that the egocentric target location might be transferred from the mPFC to the SPL via the MTL.

## Discussion

In this study, we examined neural representations of space defined by three objects and found that both the HPC and mPFC represented the object-based space around the participants. Interestingly, the HPC represented the object-based map when the participants locate their self-body in the environment constructed by the three objects, while the mPFC represented the map when the participants remembered the location of a target object relative to the self-body. These results suggest that the cognitive maps in different brain regions play different functional roles. In addition, during the targeting period, we found differential spatial representations across the MTL and mPFC: the MTL generally reinstated allocentric self-location, while the mPFC represented egocentric target location relative to self-location. Increased functional connectivity was observed between the MTL and mPFC under the necessity of the retrieval of the target location from the stored memory (targeting period) compared to when they actually faced the reference object to locate their self-body (facing period). These results suggest that mental representations of the external world formed by the coherent space and its constituent elements may be shared in the default-mode network including the MTL and mPFC. The special role of the mPFC in this scheme might be to select the object location based on the mnemonic information including the cognitive map and current self-location on it, which might be propagated from the MTL.

To examine the representation of spatial "*maps*" (Fig. 1b), the present task was designed to cancel out effects of a particular encoding experience related with the walking direction as well as a particular object identity that the participants viewed during the facing and targeting periods in each trial by balancing number of trials with each of those confounding factors in each map (see Methods). Therefore, the neural representation of the map information revealed by the RSA could not be explained by perceptual information in the present study. Moreover, the participants always stood on the center of the virtual

333 environment during the facing and targeting periods, during which the map effect was
334 examined. Because of this task design, the map information does not directly indicate self-
335 location information like place fields of place cells in the HPC (O'Keefe and Dostrovsky,
336 1971). On the other hand, the representations of place-fields are reportedly influenced by the
337 animal's cognitive map, and the existence of cognitive maps could be most clearly
338 demonstrated by a phenomenon known as "remapping", which reportedly occurs in
339 populations of place cells in the rodent HPC (Moser et al., 2017). Therefore, it might be
340 reasonable to interpret the map representations in the left mHPC during the facing period as
341 experimental evidence of "remapping" of place cells in the human HPC even though the
342 participants stood in the same position. However, holding this interpretation predicts that
343 human place cells are localized in the left mHPC. This prediction is against consistent
344 evidence from previous human studies reporting that the right HPC was more involved in
345 encoding and retrieving spatial information than the left HPC (Abrahams et al., 1997;
346 Maguire et al., 1997; Ekstrom et al., 2003; Doeller et al., 2008; Schinazi, 2013). The other
347 possible interpretation for the map representation in the left mHPC is that it may encode an
348 allocentric spatial relationship of the three objects itself. This interpretation is consistent with
349 previous human imaging studies reporting contributions of the left HPC to the imagination of
350 visual scenes, which could be constructed from multiple spatial elements (Addis et al., 2007;
351 Bird et al., 2010). The specific role of the left HPC in relational memory was also reported in
352 non-spatial information domains, including associative learning (Kumaran et al., 2009;
353 Suarez-Jimenez et al., 2018) and social interactions (Tavares et al., 2015;). Taken together, it
354 might be more reasonable to interpret that the clusters in the left mHPC was related to a
355 coherent space constructed by the multiple objects rather than its influence on representations
356 of individual spatial elements such as self-location or head direction. RSA also suggested the
357 involvement of the PRC and PHC in MTL signaling the object identity and egocentric view

358 of their spatial layout, respectively, which might be used for constructing the coherent map
359 from its constituents in the left mHPC. Future studies should address how the coherent map
360 can be constructed by multiple objects in the MTL.

361 In contrast to the facing period, the representation of the map information was found
362 in the mPFC but not in the HPC during the targeting period. In addition, the mPFC signaled
363 the egocentric location of a targeting object, while the MTL concurrently signaled the
364 allocentric self-location. Involvement of the mPFC in constructing goal-directed information
365 in the current context is consistent with accumulating evidence showing that the mPFC
366 contributes to decision making or action selection (Saxena et al., 1998; Gallagher et al., 1999;
367 Feierstein, 2006; Spiers and Maguire, 2007; Kable and Glimcher, 2009; Young and Shapiro,
368 2011; Balaguer et al., 2016; Yamada et al., 2018). These previous studies consistently
369 supported the notion that the mPFC function becomes obvious when an appropriate selection
370 requires mnemonic information in addition to incoming perceptual information (Bradfield,
371 2015). In this study, together with perceptual information responsible for target object
372 identity, mnemonic information such as the map information and allocentric self-location was
373 required to solve the task. Considering that the MTL could provide all the necessary
374 mnemonic information, a reasonable interpretation is that the mPFC was involved in the
375 selection of a target location among alternatives rather than the recollection or generation of
376 it.

377 In addition to the HPC and mPFC, the map information has been observed in other
378 brain areas such as the angular gyrus (Seghier, 2013; Price et al., 2016), lateral temporal
379 gyrus (Karnath, 2001; Himmelbach et al., 2006), and precuneus (Cavanna and Trimble, 2006)
380 that also belong to the default-mode network. The brain areas in the default-mode network,
381 particularly the MTL sub-regions except for the PRC represented allocentric self-location

382 during the targeting period. On the other hand, RSA analysis showed that widely-distributed
383 brain regions were involved in the representation of the egocentric target object location not
384 only in the default-mode network but also in the dorsal attention network and frontoparietal
385 control network. The positive and negative functional connectivity between the dorsal
386 attention network and the MTL and mPFC suggest that the egocentric target location signal is
387 transmitted from the mPFC to the brain regions of the dorsal attention network, such as the
388 SPL (Evans et al., 2016), via the MTL, which implies a pivotal functional role of MTL as a
389 hub of mental representation of object signals.

390 Interestingly, the frontoparietal control network showed a strong negative correlation
391 with both the MTL and mPFC during both the facing and targeting periods, although the
392 lPFC in the frontoparietal control network represented both the map information and
393 egocentric direction during the targeting period. In addition, the lPFC represented walking
394 direction as well as character identity during both periods. These results suggest that the lPFC
395 computes the target location independently of the default-mode network. The parallel
396 contributions of the lPFC and MTL-mPFC in choosing the target location may reflect their
397 different cognitive functions (Jimura et al., 2004). lPFC has long been considered as a center
398 of executive functions (Funahashi, 2017; Miller et al., 2018) equipped with working memory
399 (Andrews et al., 2011; Barbey et al., 2013; Brunoni and Vanderhasselt, 2014; Funahashi,
400 2017). In human fMRI studies, the lPFC has been shown to contribute to the retrieval of task-
401 relevant information when more systematic thinking is required (Epstein et al., 2017; Javadi
402 et al., 2017). In the present study, the behavioral task was designed to ensure participants
403 neither actively maintained a spatial configuration of the human characters during the
404 walking period nor any systematic strategy to solve the task, which was confirmed by the
405 post-scanning test results. The greater signal for the cognitive map and the egocentric target
406 location in the mPFC than that in the lPFC may reflect that the current spatial memory task

407 was enough easy to allow participants to depend only on the involuntary encoding and
408 subsequent memory retrieval for their top-ceiling performance (Epstein et al., 2017; Javadi et
409 al., 2017).

410 In contrast to previous memory/navigation studies, which examined brain functions
411 using spatial environments consisting of immobile landmarks (e.g., stores) and/or landscapes
412 (e.g., mountains) (Bird et al., 2010; Woollett and Maguire, 2011; Schinazi et al., 2013;
413 Chadwick et al., 2015; Brown et al., 2016), the present study used a spatial environment
414 constructed by only mobile objects that could become targets and references of self-location
415 as well as determine the space (i.e., map) around oneself. This task design allowed us to
416 extract a mental representation of the spatial environment consisting of the minimum
417 essential constituents. This reductionist method could be useful for future studies
418 investigating the construction and functional mechanisms of a cognitive map because of its
419 simplicity. One critical concern might be whether the findings discovered by this reductionist
420 method can be applied to a more complicated cognitive map consisting of large numbers of
421 immobile spatial elements, which could be learned through extensive explorations over a
422 long time period (e.g., the city of London) (Woollett and Maguire, 2011). Another related
423 concern might be whether our brain system holds only one cognitive map or multiple ones at
424 a time (Meister and Buffalo, 2018). For example, we may hold an object-based cognitive map
425 consisting of relevant mobile objects such as same species, predators, and foods, while we
426 may also hold the other cognitive map consisting of landmarks, landscapes and other
427 immobile objects such as trees. Future studies should address the relationships of different
428 types of cognitive maps (e.g., mobile vs immobile, short-term vs. long-term) and their
429 underlying neural mechanisms.

430 The present study found neural representations of the space specified by objects
431 around us. This object-based cognitive map seems to interact with representation of self-

location in HPC and to mediate a selection of egocentric target-location in mPFC, which would serve for leading us to the goal position. In addition to the spatial navigation, an existence of the object-based cognitive map may equip us with a space representation for persons separately from the background, which may serve for our social interactions (Damasio et al., 1994; Stolk et al., 2015) as well as the encoding and retrieval of episodic memory (Tulving, 2002; Squire and Wixted, 2011).

## Supplemental Information

Supplemental Information includes six figures, two tables and two videos. The videos contain trial examples for Day 1 and Day 2. In the video of day 1, please note we only used examples of correct trials in which a green square of line was preented as feedback after the participant's response. File size: 21.5 MB; Video duration: 1.23 minute; File format: .mp4; Video codec: H.264; Aspect ratio: 1024 x 768.

## Author Contributions

B.Z. and Y.N made the experimental design; B.Z. conducted all experiments and data analysis under supervision of Y.N.; B.Z. and Y.N. wrote the paper.

## Acknowledgments

The present study was funded by National Natural Science Foundation of China Grant 31421003 (to Y.N.). Computational work was supported by resources provided by the High-performance Computing Platform of Peking University. We thank Li Sheng and Sun Pei for

helpful discussions, we also thank Arielle Tambini, Lusha Zhu, Koji Jimura, Rei Akaishi and Cen Yang for comments on an early version of the manuscript.

# Main figures

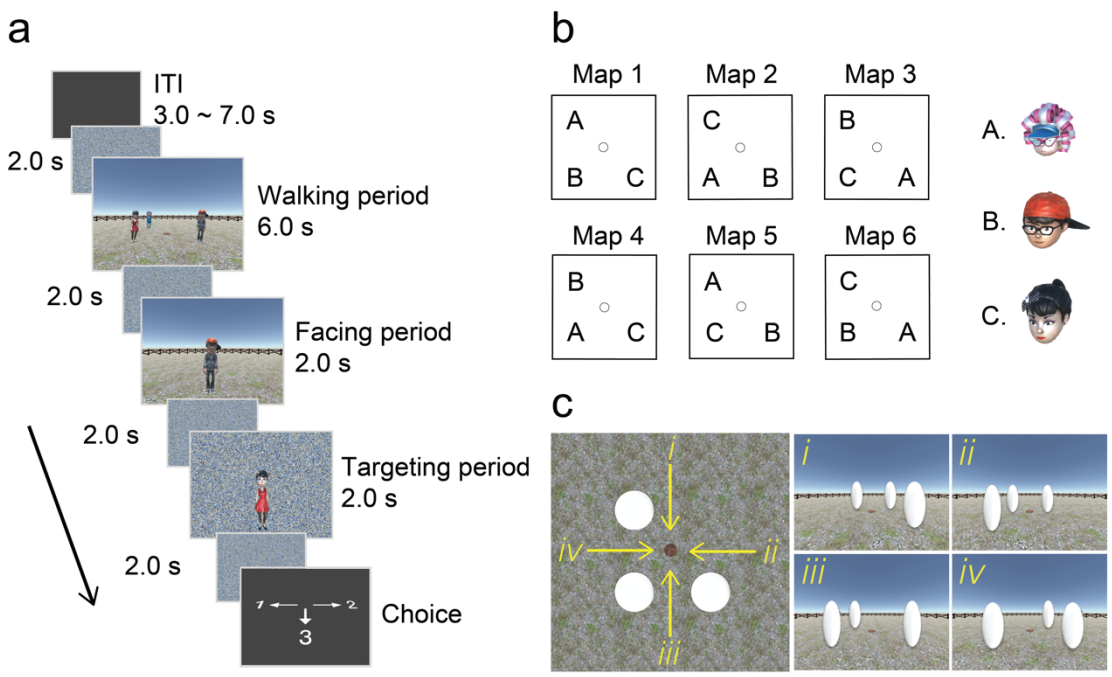


Figure 1: Task design. (a) spatial-memory task. Each trial consisted of three periods. In the walking period, participants walked toward three human characters using the first-person perspective and stopped on a wood plate. In the facing period, one of the human characters was presented, indicating the participant's current self-orientation. In the targeting period, a photo of another character was presented on the scrambled background. The participants chose the direction of the target character relative to their body upon presentation of a response cue. (b) Maps were defined by the relative position of the three human characters, while the unfilled dot represents the wood plate. (c) The walking directions were defined by the spatial layout of the three human characters from the participant's first-person perspective.

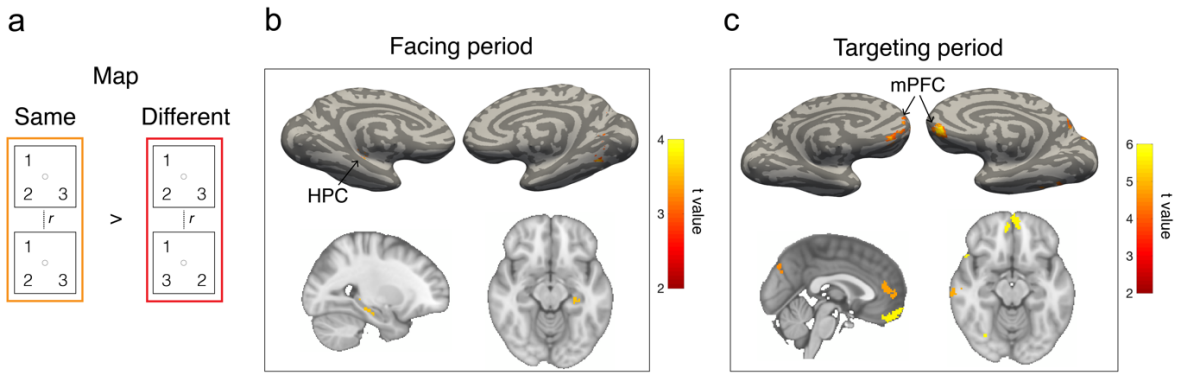


Figure 2: Neural representation of the map information in MTL and mPFC. (a) Schematic representation of decoding the cognitive map using RSA. (b) In the facing period, RSA revealed a cluster in the left middle HPC (mHPC; MNI coordinates: -28,-27,-16; shown on sagittal and transverse section) within the MTL ($P < 0.01$, initial threshold; $P < 0.05$, cluster-corrected for multiple comparison). (c) In the targeting period, clusters were revealed in the mPFC but not in the MTL ($P < 0.001$, initial threshold; $P < 0.05$, cluster-corrected for multiple comparison). A peak was revealed in the rectus within the mPFC (t value: 5.62; MNI coordinates: 4, 50, -18).

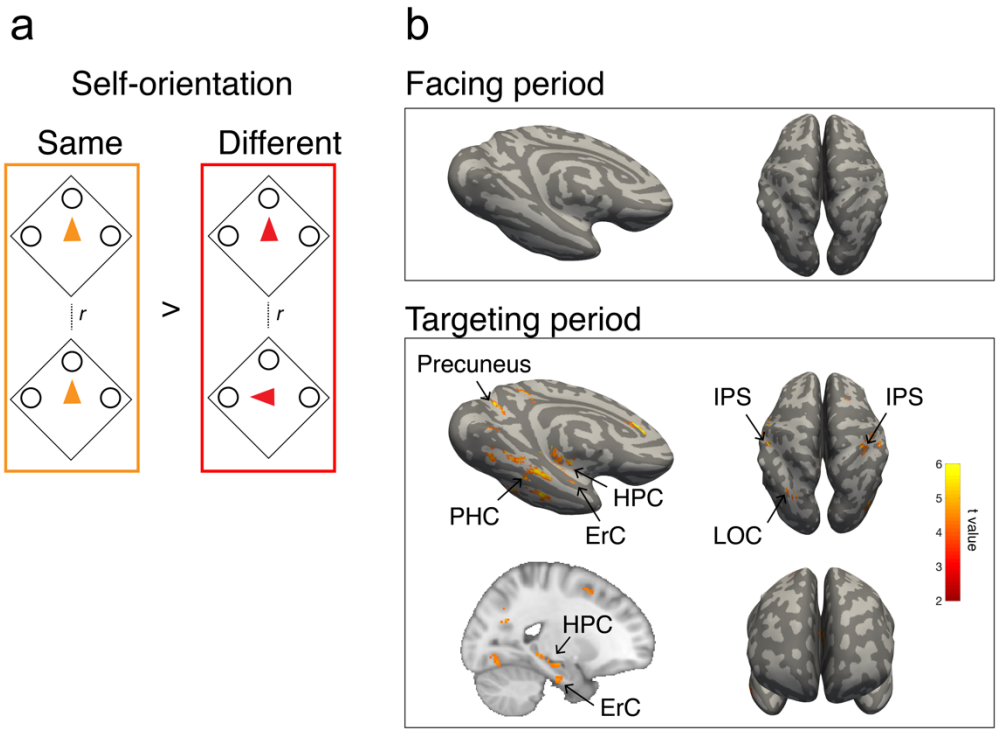


Figure 3: Neural representation of self-orientation on cognitive map. (a) Schematic representation of decoding participants' self-orientation. (b) In the facing period, no cluster was revealed even with the use of a more liberal threshold ($P < 0.01$, initial threshold; $P < 0.05$, cluster-corrected for multiple comparison). In the targeting period, clusters were revealed in the MTL (bilateral HPC, PHC, and left ErC) and self-motion areas (inferior parietal cortex, RSC, and lateral occipital cortex).

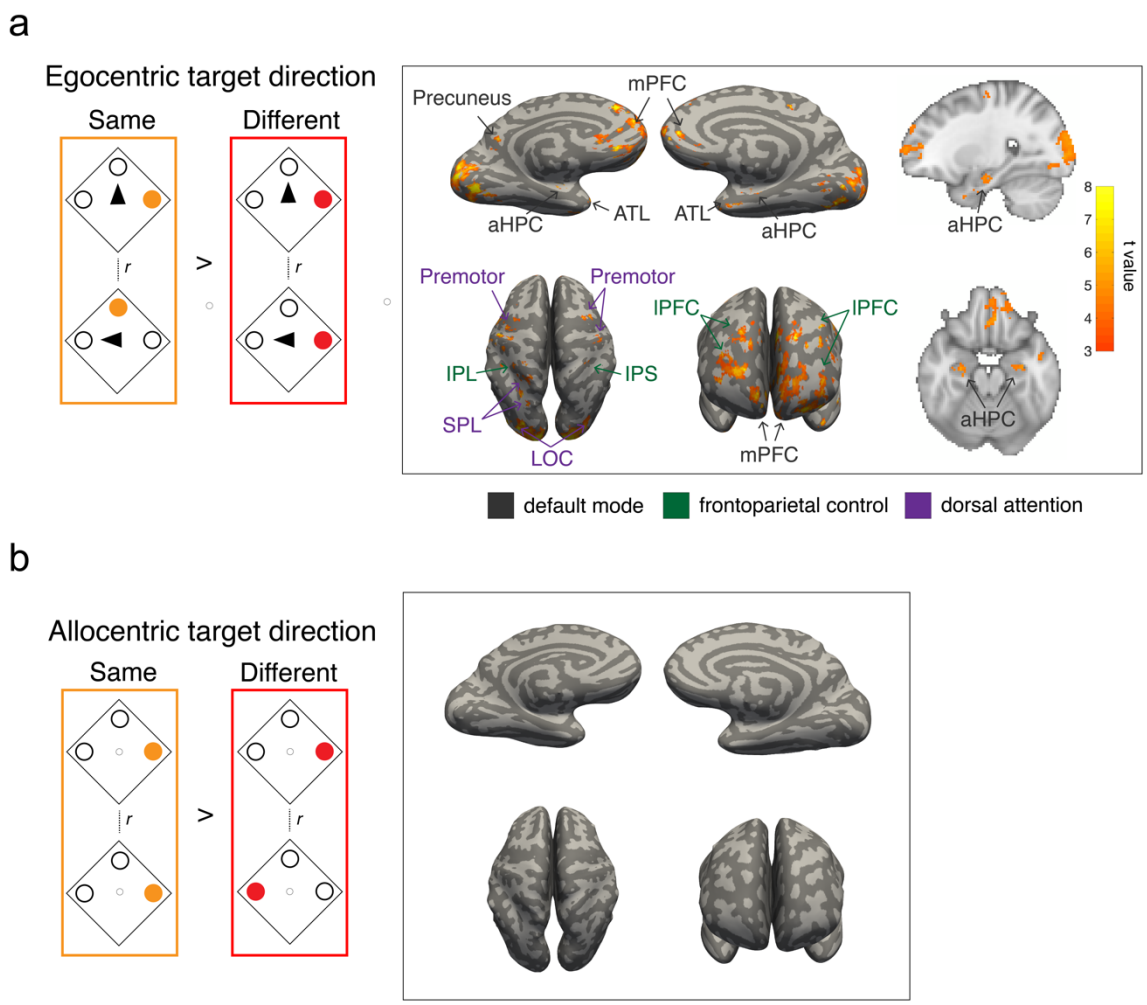


Figure 4: Neural representation of retrieved egocentric target location. (a) Left panel: Schematic representation of decoding the egocentric direction of a target character. Right panel: Clusters were revealed across a wide range of brain areas ($P < 0.001$, initial threshold; $P < 0.05$, cluster-corrected for multiple comparison). Many of the clusters belonged to one of the following three functional networks: the default-mode network, frontoparietal control network, and dorsal attention network. The aHPC is shown on sagittal and transverse section of volumn image for display purpose ($P < 0.001$, initial threshold; $P < 0.05$, cluster-corrected for multiple comparison). (b) Left panel: Schematic representation of decoding allocentric direction of a target character . Right panel: No clusters were revealed even with the use of a liberal threshold ($P < 0.01$, initial threshold; $P < 0.05$, cluster-corrected for multiple comparison).

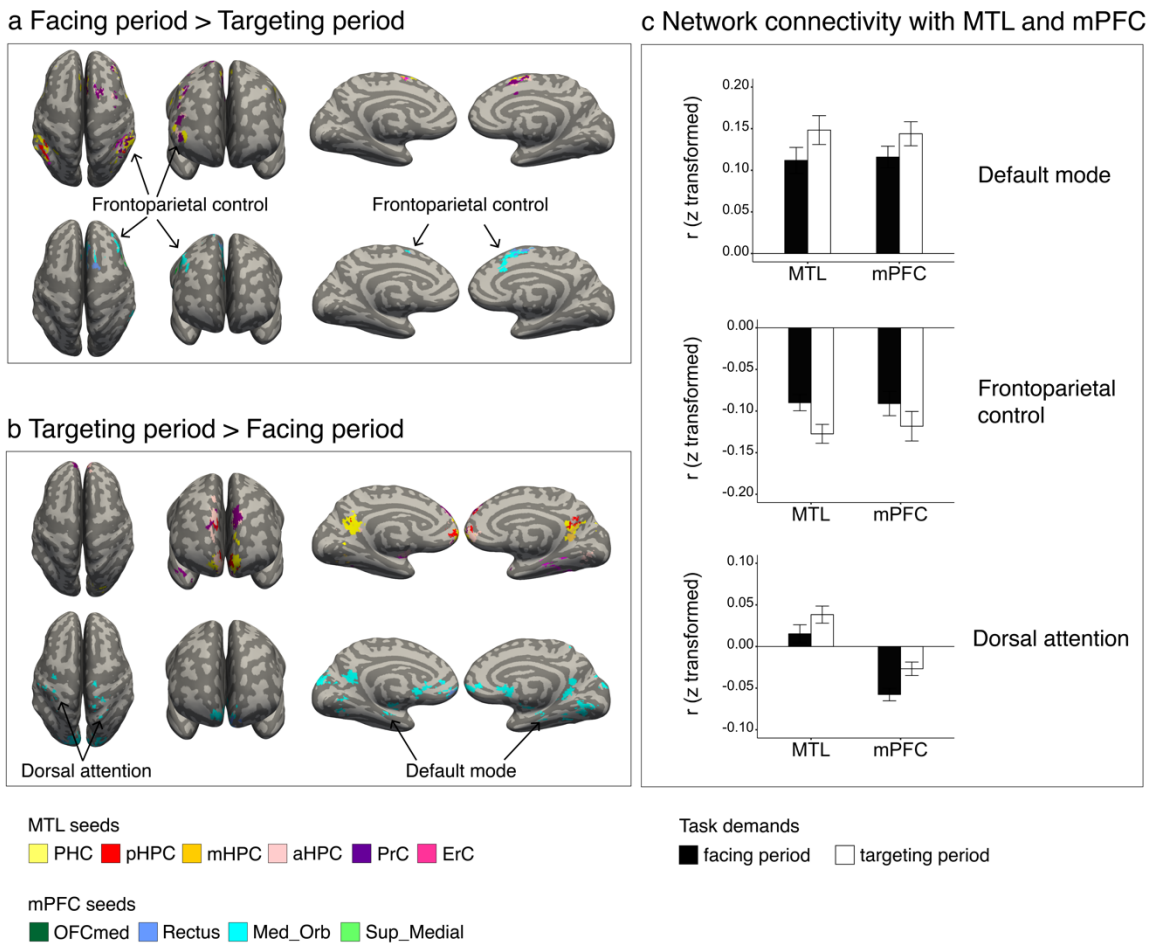


Figure 5: Increased default-mode network connectivity while locating a target compared with locating oneself. (a) The frontoparietal control network showed enhanced connectivity strength with the MTL and mPFC in the facing period compared to the targeting period ($P < 0.001$, initial threshold; $P < 0.05$, cluster-corrected for multiple comparison). (b) The default-mode network and dorsal attention network showed enhanced connectivity strength with the MTL and mPFC in the targeting period compared to the facing period ($P < 0.001$, initial threshold; $P < 0.05$, cluster-corrected for multiple comparison). (c) The mean connectivity strength of MTL and mPFC sub-regions with three networks, respectively. Note that the connectivity between default-mode network and MTL/mPFC was examined using default-mode network mask without the MTL/mPFC, respectively.

## Methods

### Participants

Nineteen right-handed university students with normal or corrected-to-normal vision were recruited from Peking University (12 females, 7 males). The average age of the participants was 24.9 years (range: 18–30 years). All participants had no history of psychiatric or neurological disorders and gave their written informed consent prior to the start of the experiment, which was approved by the Research Ethics Committee of Peking University.

### Task design

*Virtual environment.* We programmed a 3D virtual environment using Unity software (Unity Technologies, San Francisco). The environment was designed with a circular fence as a boundary (48 virtual meters in diameter), a flat grassy ground, a uniform blue sky, and with a wood plate surrounded by four vertices of a square placed in the center (Fig. 1b, 4.7 virtual meters for side length). Three human characters (Mixamo, San Francisco, https://www.mixamo.com) were placed on three of the vertices in each trial. A map was defined by the relative relationship of the three human characters (Fig. 1b). From the six possible maps, three of them were pseudo-randomly selected for each participant to collect enough number of trials' data for each condition during the allowable range of scanning duration. The maps were the only environmental cues relevant to the task requirement, no distal cues were used outside the boundary. Participants performed the task using the first-person perspective with a 90° field of view (aspect ratio = 4:3), they had never seen a top-down view of the virtual environment.

*Walking period.* Participants walked from one of four starting locations near the circular boundary (4 virtual meters from the boundary) toward the human characters (Fig. 1c) and

533 stopped on the wood plate. The visual stimuli (spatial environment viewed from first-person
534 perspective) were determined by the combination of the map and walking direction, in other
535 words, each map was presented by four different visual stimuli that were determined by the
536 starting position (Fig. 1c). Importantly, participants were blinded to the map concept
537 throughout the task. The walking period lasted for 6.0 s, during which each character had a
538 20.6% probability of nodding its head at a random time point between the start and end of
539 walking. There was a 50%, 38.9%, 10.2%, and 0.9% probability for 0, 1, 2, and 3 characters
540 to nod head in each trial; we subjectively selected a 20.6% head-nodding probability for each
541 character to ensure an approximately equal number of trials with head-nodding and no head-
542 nodding. During the walking period, participants were required to pay attention to the heads
543 of the human characters rather than to memorize their spatial arrangement. The height of the
544 participants was 1.8 virtual meters from the ground, which was the same as that of the human
545 characters. No response was required during the walking period.
546 Two tasks were completed in two consecutive days. On day 1, the participants
547 performed an HND task that did not include spatial-memory trials. On day 2, participants
548 performed a spatial-memory task.

549 *Head-nodding detection (HND) task.* Participants performed 144 randomly ordered HND
550 trials in a behavioral experimental room. In each trial, a photo of one of the characters was
551 presented on a screen after the walking period, and participants were asked to indicate
552 whether the character nodded its head or not (Fig. S1a). For this task, there was a 50% chance
553 that the character in the presented photo nodded its head. Feedback was given after the
554 participants had responded with either green (correct) or red (incorrect) photo border. The
555 stimuli were rendered on a PC and presented on a 27-inch LCD monitor (ViewSonic
556 XG2730) with a screen resolution of 1024 x 768. The HND task was used to examine
557 whether participants paid attention to head-nodding rather than memorizing the spatial

558 arrangement of the characters, which would be indicated by high success rates in the head-
559 nodding test.

560 *Spatial-memory task.* During this task, participants performed 144 spatial-memory
561 trials (90%) and 16 HND trials (10%) that lasted ~ 70 min in an MRI scanner. Participants
562 were notified that the remuneration depended only on the performance in the HND trials
563 although they were also encouraged to perform the spatial memory task as best as they could
564 (videos of trial examples are available online for both tasks). The trial-type (i.e., HND or
565 memory task) was distinguishable after the walking period by subsequent stimuli. In the
566 spatial-memory task, participants experienced a "facing period" and a "targeting period"
567 sequentially after the walking period. In the facing period, their self-orientation was changed
568 immediately to one of the human characters (facing-character) without viewpoint transition,
569 and a character with the environment background was presented for 2.0 s with the other two
570 characters being invisible, the participants were instructed to face the character. In the
571 targeting period, a photo of another character (targeting-character) was presented as a target
572 on a scrabbled background for 2.0 s. Each of the three experimental periods was followed by
573 a 2.0-s delay (noise screen). At the end of each trial, participants indicated the direction of the
574 target character relative to their self-body by pressing a button when a cue presented on the
575 screen; no feedback was shown for both trial-types (Fig. 1a). The spatial-memory task
576 contained four experimental sessions, each containing a spatial information combination of 3
577 maps x 4 walking directions x 3 facing-character identities in each session, with targeting-
578 characters balanced across sessions. After scanning, all participants completed a post-
579 scanning interview and reported the strategy they used to perform the task (Table. S2).
580

581 **fMRI data acquisition**

582 Imaging data were collected using a 3T Siemens Prisma scanner equipped with a 20-channel
583 receiver head coil. Functional data were acquired with a Multi-band Echo Planer imaging
584 (EPI) sequence (TR = 2000 ms, TE = 30 ms, matrix size: 112 × 112 x 62, flip angle: 90°, gap
585 = 0 mm; resolution: 2 × 2 × 2.3 $mm^3$, number of slices: 62, slice thickness: 2 mm, slice
586 orientation: transversal), four experimental sessions were collected with, on average, 478,
587 476, 473, 475 TRs, respectively. A high-resolution T1-weighted three-dimensional
588 anatomical data set was collected to aid in registration (MPRAGE, TR = 2530 ms, TE = 2.98
589 ms, matrix size: 448 x 512 x 192, flip angle: 7°, resolution: 0.5 × 0.5 × 1 $mm^3$ , number of
590 slices: 192, slice thickness: 1 mm, slice orientation: sagittal). During scanning, experimental
591 stimuli were presented through a Sinorad LCD projector (Shenzhen Sinorad Medical
592 Electronics) onto a 33-inch rear-projection screen located over the subject's head with a
593 resolution of 1024 x 768 and viewed with an angled mirror positioning on the head coil.
594
595 **fMRI preprocessing**
596 Functional data for each session were preprocessed independently using FSL FEAT
597 (FMRIB's Software Library, version 6.00, https://fsl.fmrib.ox.ac.uk/fsl/fslwiki; Woolrich et
598 al., 2001; Woolrich et al., 2004). For each session, the first three functional volumes were
599 discarded to allow for T1 equilibration, and the remaining functional volumes were slice-time
600 corrected, realigned to the first image, and high-pass filtered at 100 s. For group-level
601 statistics, each session's functional data were registered to a T1-weighted standard image
602 (MNI152) using FSL FLIRT (Jenkinson and Smith, 2001), and this procedure also resampled
603 the functional voxels into a 2 x 2 x 2 mm resolution. For RSA, data were left unsmoothed to
604 preserve any fine-grained spatial information (Chadwick et al., 2012). For functional
605 connectivity analysis, data were smoothed using a 5 mm FWHM Gaussian kernel and were
606 high-pass filtered at 0.01 Hz to remove low-frequency signal drifts.

607

608 **Anatomical masks**

609 We manually delineated the MTL, including the HPC, PHC, PRC, and ERC on each
610 participant's native space using established protocols (Insausti et al., 1998; Pruessner et al.,
611 2000; Pruessner et al., 2002; Duvernoy, 2005), as well as a delineating software ITK-SNAP
612 (www.itksnap.org). The HPC was further divided into its anterior, middle, and posterior parts
613 given the anatomical and functional variability along the HPC long axis (Poppenk et al.,
614 2013), the anterior border of pHPC and the posterior border of aHPC were defined by the
615 appearance of the crus of the fornix and the uncal apex relative to mHPC along the coronal
616 orientation, respectively (Pruessner et al., 2000; Poppenk et al., 2013). For PFC sub-regions,
617 we used the AAL template (Rolls et al., 2015), and selected four mPFC sub-regions for ROI-
618 analysis, which included the rectus, medial orbital gyrus (OFCmed), medial orbital frontal
619 gyrus (Med_Orb), and superior medial frontal gyrus (Sup_Med). All ROIs were resampled
620 and aligned with the functional volumes, and voxels outside of the brain were excluded.

621

622 **Representational similarity analysis (RSA)**

623 Task-relevant information was decoded using RSA. We tried to dissociate the neural effect of
624 facing and targeting period based on 4 s duration from each period onset to the end of
625 following noise period (Zeithamova et al., 2017). First, the trial-based multi-voxel activity
626 patterns of two periods were obtained by creating two separate univariate general linear
627 models (GLM). In each GLM, the 4 s blood-oxygen-level-dependent (BOLD) signals of 36
628 trials (a session) were modeled using boxcar regressors. In addition to the 36 trial-based
629 regressors of interest, nuisance regressors were included, which included twelve regressors
630 for modeling the visual patterns of the walking period determined by the maps and walking
631 directions, three for modeling the character identities in the remaining period (for example, in

632 the facing period GLM, three targeting characters were specified as nuisance regressors
633 rather than the facing characters), four for modeling head-nodding detection trials, three for
634 modeling 3 directional cues in the response period, and six motion parameters. This
635 procedure generated 36 trial-based multi-voxel patterns in participant's native space (2 x 2 x
636 2.3 mm voxels) for each period, those multi-voxel patterns were normalized prior to
637 subsequent analysis by subtracting the grand mean pattern of the 36 multi-voxel patterns for
638 each session (Vass and Epstein, 2013).
639 Searchlight-based RSA. Next, we computed the representational similarity for each spatial
640 information based on the multi-voxel patterns using a searchlight-based RSA (Libby et al.,
641 2014; Chadwick et al., 2015), which was conducted using custom Matlab (version R2018b,
642 www.mathworks.com/matlab/) scripts. In detail, a sphere with a 6 mm radius was constructed
643 (85 voxels per sphere) for each brain voxel, and the spheres near the edge of the brain with
644 fewer than ten voxels were excluded from the analysis. The activity parameters within each
645 sphere were extracted from each of the 36 multi-voxel patterns, resulting in a 36-column by
646 n-row (number of voxels within the sphere) matrix. The pattern similarity was then calculated
647 between each column-by-column pair using Pearson's correlation, and was normalized using
648 Fisher's r-to-z transformation. This procedure finally generated a 36-by-36 correlation matrix
649 for each period in each brain voxel. Next, given that a multi-voxel pattern contains the
650 combination of multiple spatial information, we conducted a GLM for each correlation
651 matrix by specifying multiple categorical regressors to rule out potential influences. Each
652 spatial representation represented specific spatial information and used either indicator "1
653 (same)" or " 0 (different)" that corresponded with the correlation coefficient of a given
654 column-to-row cell of the correlation matrix. For the facing period, the GLM contained five
655 categorical regressors, which included the (1) "map", (2) "walking direction", and (3)
656 "facing-character identity". Since the participants reported thinking about their bodies

657 rotating between the walking direction and self-orientation relative to the environment, we
658 also added the (4) "rotation angle" (turn left/right 45°, turn left/right 135°), and (5) their
659 "self-orientation" into the GLM. For the targeting period, seven regressors were built, which
660 included: (1) "map", (2) "walking direction", (3-4) participants' "rotation angle" and "self-
661 orientation", (5) "targeting-character identity", and (6-7) "egocentric and allocentric position
662 of target-character". It is important to note that the "facing-character identity" was not
663 included in the targeting period GLM since the effect of each facing character was regressed
664 out in the GLM computing of multi-voxel activity patterns. $r^2$ was computed and ranged from
665 0 to 0.03 for the facing period GLM, and 0 to 0.04 for the targeting period GLM (Table S1).
666 Each regressor's parameter was then assigned to the center voxel of each sphere so that a
667 whole-brain statistical parametric mapping could be generated for each spatial information
668 for each period, with those spatial representations being finally averaged across the four
669 scanner sessions. By using this method, spatial information should be successfully decoded if
670 the regressors stably predict the correlation coefficients in any voxels.
671
672 *ROI-based RSA*. To validate the spatial representations, we further conducted an
673 independent RSA using anatomical ROIs of MTL and PFC sub-regions. We reasoned that
674 since searchlight analysis identifies the spatial representations as clusters in small portions of
675 anatomical regions, if those representations are stable enough, the corresponding anatomical
676 regions, on average, should show a clear increasing tendency in similarity when spatial
677 information between trial-pairs are similar compared to different such that they match the
678 searchlight results. To test this, we separated each ROI into the left and right hemispheres and
679 generated 20 anatomical masks (Fig. S4a; 12 for the MTL and 8 for the mPFC). The mPFC
680 masks were normalized into the participants' native space. The RSA procedure for each ROI
681 was similar to searchlight analysis, which produced a 36-by-36 correlation matrix for each

682 period. Next, for each spatial information (e.g., map), the correlation matrix elements were z-
683 transformed and were grouped into "same" and "different" conditions. The mean values of
684 the matrix elements in the same condition was subtracted by those in the different condition
685 in each session (36 trials). The subtracted values were averaged across the four sessions for
686 each participant. We referred to this averaged value as a discrimination score. We tested
687 whether or not the discrimination score was positive among the participants using one-sample
688 t-test (one-tail).

689 **Functional connectivity (FC) analysis**

690 To investigate the functional networks for different task demands, we examined the whole-
691 brain FC using each sub-region of MTL and mPFC as seed (Fig. S4a; 12 for the MTL and 8
692 for the mPFC). In detail, we first removed the nuisance covariates from the preprocessed
693 functional data by creating a GLM, which specified the signal averaged over the lateral
694 ventricles, white matter, and whole brain, six motion parameters, and their derivatives as
695 regressors. The residual signal was bandpass-filtered, leaving signals within the frequency
696 range 0.01 to 0.1 Hz, and was shifted by two TR intervals (4 s) for subsequent analysis
697 (Tompary and Davachi, 2017). We computed a regional time course for each anatomical
698 mask in each of facing and targeting period. To do this, we averaged signals over the mask at
699 each TR within the period, and then concatenated the two values in one trial with those in the
700 next trial within a session (Ranganath et al., 2005). The regional time course for each
701 anatomical mask was correlated with the time course of each voxel in the rest of the brain,
702 resulting in a whole-brain correlation map for each period in each scanning session. The
703 correlation maps were averaged across four scanning sessions for each participant, and were
704 then submitted to a two-tailed t-test for group level statistics.

705 Each cluster, which derived from the contrast analysis in connectivity between facing
706 and targeting period based on an initial threshold of p=0.001, was assigned to each of the

three networks based on previous literatures: default-mode network, frontoparietal control network, and dorsal attention network (Vincent et al., 2008; Schacter et al., 2012; Gelström and Graziano., 2017). In the present study, default-mode network contains the clusters of mPFC, MTL, posterior cingulate cortex, and anterior temporal gyrus; frontoparietal control network contains the clusters of paracingulate gyrus, lateral PFC, and inferior parietal lobule; dorsal attention network contains the clusters of occipital pole, lateral occipital cortex, cuneal cortex, lingual gyrus, superior parietal lobule, and postcentral gyrus (Fig. S4b). To examine modulation effects on the connectivity of MTL/mPFC with the large-scale networks by different task demands, we computed mean connectivity between each of MTL and mPFC subregions with each network. For the default-mode network, we prepared for two masks, in which the MTL or mPFC was removed for the examinations of its connectivity with the default-mode network.

**Statistics**

For searchlight-based RSA, we used an initial threshold of $p < 0.001$. If no clusters were revealed, a more liberal threshold of $p < 0.01$ was used. For whole brain FC analysis, an initial threshold of $p<0.001$ was used to identify robust network patterns. For both searchlight-based RSA and whole brain FC analysis, the reliability of significant effects was tested using a non-parametric statistical inference that does not make assumptions about the distribution of the data, the test was conducted with the FSL randomise package (version v2.9, http://fsl.fmrib.ox.ac.uk/fsl/fslwiki/Randomise) (Nichols and Holmes, 2002; Winkler et al., 2014) using 5000 random sign-flips and threshold-free clustering. We then reported voxels that were significant at $p < 0.05$ after correcting for multiple comparisons across the entire brain. ROI-based RSA used one-tailed one sample t-test to examine the significance of each anatomical mask. Paired t-test was used to examine the difference in connectivity

among MTL and mPFC subregions between task demands. All t-test results were Bonferroni-corrected for multiple comparison (alpha < 0.05). Analysis of variance (ANOVA) was used to test the influence in connectivity between MTL/mPFC and large-scale functional network along time periods.

## Reference


Abrahams, S., Pickering, A., Polkey, C. E., & Morris, R. G. (1997). Spatial memory deficits in patients with unilateral damage to the right hippocampal formation. Neuropsychologia, 35(1), 11-24.

Andrews, S. C., Hoy, K. E., Enticott, P. G., Daskalakis, Z. J., & Fitzgerald, P. B. (2011). Improving working memory: the effect of combining cognitive activity and anodal transcranial direct current stimulation to the left dorsolateral prefrontal cortex. Brain stimulation, 4(2), 84-89.

Addis, D. R., Wong, A. T., & Schacter, D. L. (2007). Remembering the past and imagining the future: common and distinct neural substrates during event construction and elaboration. Neuropsychologia, 45(7), 1363-1377.

Barbey, A. K., Koenigs, M., & Grafman, J. (2013). Dorsolateral prefrontal contributions to human working memory. cortex, 49(5), 1195-1205.

Brunoni, A. R., & Vanderhasselt, M. A. (2014). Working memory improvement with non-invasive brain stimulation of the dorsolateral prefrontal cortex: a systematic review and meta-analysis. Brain and cognition, 86, 1-9.

Bird, C. M., Capponi, C., King, J. A., Doeller, C. F., & Burgess, N. (2010). Establishing the boundaries: the hippocampal contribution to imagining scenes. Journal of Neuroscience, 30(35), 11688-11695.

Buffalo, E.A. (2015). Bridging the gap between spatial and mnemonic views of the hippocampal formation. Hippocampus *25*, 713-718.

Balaguer, J., Spiers, H., Hassabis, D., & Summerfield, C. (2016). Neural mechanisms of hierarchical planning in a virtual subway network. Neuron, 90(4), 893-903.

Bradfield, L. A., Dezfouli, A., van Holstein, M., Chieng, B., & Balleine, B. W. (2015). Medial orbitofrontal cortex mediates outcome retrieval in partially observable task situations. Neuron, 88(6), 1268-1280.

Brown, T. I., Carr, V. A., LaRocque, K. F., Favila, S. E., Gordon, A. M., Bowles, B., ... & Wagner, A. D. (2016). Prospective representation of navigational goals in the human hippocampus. Science, 352(6291), 1323-1326.

Cavanna, A.E., and Trimble, M.R. (2006). The precuneus: a review of its functional anatomy and behavioural correlates. Brain : a journal of neurology 129, 564-583.

Campbell, K.L., Madore, K.P., Benoit, R.G., Thakral, P.P., and Schacter, D.L. (2018). Increased hippocampus to ventromedial prefrontal connectivity during the construction of episodic future events. Hippocampus 28, 76-80.

Chadwick, M. J., Jolly, A. E., Amos, D. P., Hassabis, D., & Spiers, H. J. (2015). A goal direction signal in the human entorhinal/subicular region. Current Biology, 25(1), 87-92.

Chadwick, M. J., Bonnici, H. M., & Maguire, E. A. (2012). Decoding information in the human hippocampus: a user's guide. Neuropsychologia, 50(13), 3107-3121.

Duvernoy, H. M. (2005). The human hippocampus: functional anatomy, vascularization and serial sections with MRI. Springer Science & Business Media.

Damasio, H., Grabowski, T., Frank, R., Galaburda, A.M., and Damasio, A.R. (1994). The return of Phineas Gage: clues about the brain from the skull of a famous patient. Science 264, 1102-1105.

Doeller, C. F., King, J. A., & Burgess, N. (2008). Parallel striatal and hippocampal systems for landmarks and boundaries in spatial memory. Proceedings of the National Academy of Sciences, 105(15), 5915-5920.

Ekstrom, A.D., Kahana, M.J., Caplan, J.B., Fields, T.A., Isham, E.A., Newman, E.L., and Fried, I. (2003). Cellular networks underlying human spatial navigation. Nature *425*, 184-188.

Eichenbaum, H. (2017). The role of the hippocampus in navigation is memory. Journal of neurophysiology 117, 1785-1796.

Epstein, R.A., Patai, E.Z., Julian, J.B., and Spiers, H.J. (2017). The cognitive map in humans: spatial navigation and beyond. Nature neuroscience 20, 1504-1513.

Evans, T., Bicanski, A., Bush, D., & Burgess, N. (2016). How environment and self-motion combine in neural representations of space. The Journal of physiology, 594(22), 6535-6546.

Feierstein, C. E., Quirk, M. C., Uchida, N., Sosulski, D. L., & Mainen, Z. F. (2006). Representation of spatial goals in rat orbitofrontal cortex. Neuron, 51(4), 495-507.

Funahashi, S. (2017). Prefrontal Contribution to Decision-Making under Free-Choice Conditions. Frontiers in neuroscience 11, 431.

Gaesser, B., Spreng, R. N., McLelland, V. C., Addis, D. R., & Schacter, D. L. (2013). Imagining the future: evidence for a hippocampal contribution to constructive processing. Hippocampus, 23(12), 1150-1161.

Gallagher, M., McMahan, R. W., & Schoenbaum, G. (1999). Orbitofrontal cortex and representation of incentive value in associative learning. Journal of Neuroscience, 19(15), 6610-6614.

Gelström, K. M., & Graziano, M. S. (2017). The inferior parietal lobule and temporoparietal junction: a network perspective. Neuropsychologia, 105, 70-83.

Himmelbach, M., Erb, M., and Karnath, H.O. (2006). Exploring the visual world: the neural substrate of spatial orienting. NeuroImage 32, 1747-1759.

Hargreaves, E.L., Rao, G., Lee, I., and Knierim, J.J. (2005). Major dissociation between medial and lateral entorhinal input to dorsal hippocampus. Science 308, 1792-1794.

Hassabis, D., & Maguire, E. A. (2007). Deconstructing episodic memory with construction. Trends in cognitive sciences, 11(7), 299-306.

Insausti, R., Juottonen, K., Soininen, H., Insausti, A. M., Partanen, K., Vainio, P., ... & Pitkänen, A. (1998). MR volumetric analysis of the human entorhinal, perirhinal, and temporopolar cortices. American Journal of Neuroradiology, 19(4), 659-671.

Javadi, A.H., Emo, B., Howard, L.R., Zisch, F.E., Yu, Y., Knight, R., Pinelo Silva, J., and Spiers, H.J. (2017). Hippocampal and prefrontal processing of network topology to simulate the future. Nature communications 8, 14652.

Jenkinson, M., & Smith, S. (2001). A global optimisation method for robust affine registration of brain images. Medical image analysis, 5(2), 143-156.

Jimura, K., Konishi, S., and Miyashita, Y. (2004). Dissociable concurrent activity of lateral and medial frontal lobe during negative feedback processing. NeuroImage *22*, 1578-1586.

Karnath, H. O. (2001). New insights into the functions of the superior temporal cortex. Nature Reviews Neuroscience, 2(8), 568.

Kumaran, D., Summerfield, J. J., Hassabis, D., & Maguire, E. A. (2009). Tracking the emergence of conceptual knowledge during human decision making. Neuron, 63(6), 889-901.

Kriegeskorte, N., Goebel, R., & Bandettini, P. (2006). Information-based functional brain mapping. Proceedings of the National Academy of Sciences, 103(10), 3863-3868.

Kriegeskorte, N., Mur, M., Ruff, D. A., Kiani, R., Bodurka, J., Esteky, H., ... & Bandettini, P. A. (2008). Matching categorical object representations in inferior temporal cortex of man and monkey. Neuron, 60(6), 1126-1141.

Kable, J.W., and Glimcher, P.W. (2009). The neurobiology of decision: consensus and controversy. Neuron *63*, 733-745.

Konishi, S., Wheeler, M.E., Donaldson, D.I., and Buckner, R.L. (2000). Neural correlates of episodic retrieval success. NeuroImage *12*, 276-286.

Libby, L. A., Hannula, D. E., & Ranganath, C. (2014). Medial temporal lobe coding of item and spatial information during relational binding in working memory. Journal of Neuroscience, 34(43), 14233-14242.

Meister, M.L.R., and Buffalo, E.A. (2018). Neurons in primate entorhinal cortex represent gaze position in multiple spatial reference frames. The Journal of neuroscience : the official journal of the Society for Neuroscience.

Miller, E. K., Lundqvist, M., & Bastos, A. M. (2018). Working Memory 2.0. Neuron, 100(2), 463-475.

Moser, E.I., Moser, M.B., and McNaughton, B.L. (2017). Spatial representation in the hippocampal formation: a history. Nature neuroscience 20, 1448-1464.

Maguire, E. A., Frackowiak, R. S., & Frith, C. D. (1997). Recalling routes around London: activation of the right hippocampus in taxi drivers. Journal of neuroscience, 17(18), 7103-7110.

McCormick, C., Ciaramelli, E., De Luca, F., and Maguire, E.A. (2018). Comparing and Contrasting the Cognitive Effects of Hippocampal and Ventromedial Prefrontal Cortex Damage: A Review of Human Lesion Studies. Neuroscience 374, 295-318.

Nakazawa, K., Quirk, M.C., Chitwood, R.A., Watanabe, M., Yeckel, M.F., Sun, L.D., Kato, A., Carr, C.A., Johnston, D., Wilson, M.A., et al. (2002). Requirement for hippocampal CA3 NMDA receptors in associative memory recall. Science 297, 211-218.

Nichols, T. E., & Holmes, A. P. (2002). Nonparametric permutation tests for functional neuroimaging: a primer with examples. Human brain mapping, 15(1), 1-25.

Naya, Y., and Suzuki, W.A. (2011). Integrating what and when across the primate medial temporal lobe. Science 333, 773-776.

Naya, Y., Yoshida, M., and Miyashita, Y. (2001). Backward spreading of memory-retrieval signal in the primate temporal cortex. Science *291*, 661-664.

O'Keefe, J., & Dostrovsky, J. (1971). The hippocampus as a spatial map: preliminary evidence from unit activity in the freely-moving rat. Brain research.

Pruessner, J. C., Li, L. M., Serles, W., Pruessner, M., Collins, D. L., Kabani, N., ... & Evans, A. C. (2000). Volumetry of hippocampus and amygdala with high-resolution MRI and three-dimensional analysis software: minimizing the discrepancies between laboratories. Cerebral cortex, 10(4), 433-442.

Pruessner, J. C., Köhler, S., Crane, J., Pruessner, M., Lord, C., Byrne, A., ... & Evans, A. C. (2002). Volumetry of temporopolar, perirhinal, entorhinal and parahippocampal cortex from high-resolution MR images: considering the variability of the collateral sulcus. Cerebral Cortex, 12(12), 1342-1353.

Packard, M.G., and McGaugh, J.L. (1996). Inactivation of hippocampus or caudate nucleus with lidocaine differentially affects expression of place and response learning. Neurobiology of learning and memory 65, 65-72.

Poppenk, J., Evensmoen, H. R., Moscovitch, M., & Nadel, L. (2013). Long-axis specialization of the human hippocampus. Trends in cognitive sciences, 17(5), 230-240.

Price, A. R., Peelle, J. E., Bonner, M. F., Grossman, M., & Hamilton, R. H. (2016). Causal evidence for a mechanism of semantic integration in the angular gyrus as revealed by high-definition transcranial direct current stimulation. Journal of Neuroscience, 36(13), 3829-3838.

Ranganath, C., Heller, A., Cohen, M. X., Brozinsky, C. J., & Rissman, J. (2005). Functional connectivity with the hippocampus during successful memory formation. Hippocampus, 15(8), 997-1005.

Ranganath, C., & Ritchey, M. (2012). Two cortical systems for memory-guided behaviour. Nature Reviews Neuroscience, 13(10), 713.

Rolls, E. T., Joliot, M., & Tzourio-Mazoyer, N. (2015). Implementation of a new parcellation of the orbitofrontal cortex in the automated anatomical labeling atlas. Neuroimage, 122, 1-5.

Redish, A.D., and Touretzky, D.S. (1998). The role of the hippocampus in solving the Morris water maze. Neural computation 10, 73-111.

Seghier, M. L. (2013). The angular gyrus: multiple functions and multiple subdivisions. The Neuroscientist, 19(1), 43-61.

Suarez-Jimenez, B., Bisby, J. A., Horner, A. J., King, J. A., Pine, D. S., & Burgess, N. (2018). Linked networks for learning and expressing location-specific threat. Proceedings of the National Academy of Sciences, 115(5), E1032-E1040.

Spiers, H. J., & Maguire, E. A. (2007). A navigational guidance system in the human brain. Hippocampus, 17(8), 618-626.

Schinazi, V. R., Nardi, D., Newcombe, N. S., Shipley, T. F., & Epstein, R. A. (2013). Hippocampal size predicts rapid learning of a cognitive map in humans. Hippocampus, 23(6), 515-528.

Squire, L.R., and Wixted, J.T. (2011). The cognitive neuroscience of human memory since H.M. Annual review of neuroscience 34, 259-288.

Schacter, D.L., Addis, D.R., and Buckner, R.L. (2007). Remembering the past to imagine the future: the prospective brain. Nature reviews Neuroscience 8, 657-661.

Spreng, R. N., & Schacter, D. L. (2011). Default network modulation and large-scale network interactivity in healthy young and old adults. Cerebral Cortex, 22(11), 2610-2621.

Schacter, D.L. (2012). Adaptive constructive processes and the future of memory. The American psychologist 67, 603-613.

Schacter, D. L., Addis, D. R., Hassabis, D., Martin, V. C., Spreng, R. N., & Szpunar, K. K. (2012). The future of memory: remembering, imagining, and the brain. Neuron, 76(4), 677-694.

Stolk, A., D'Imperio, D., di Pellegrino, G., and Toni, I. (2015). Altered communicative decisions following ventromedial prefrontal lesions. Current biology : CB 25, 1469-1474.

Saxena, S., Brody, A. L., Schwartz, J. M., & Baxter, L. R. (1998). Neuroimaging and frontal-subcortical circuitry in obsessive-compulsive disorder. The British Journal of Psychiatry, 173(S35), 26-37.

Suzuki, W., and Naya, Y. (2011). Two routes for remembering the past. Cell *147*, 493-495.

Suzuki, W.A., and Naya, Y. (2014). The perirhinal cortex. Annual review of neuroscience *37*, 39-53.

Tolman, E. C. (1948). Cognitive maps in rats and men. Psychological review, 55(4), 189.

Tavares, R. M., Mendelsohn, A., Grossman, Y., Williams, C. H., Shapiro, M., Trope, Y., & Schiller, D. (2015). A map for social navigation in the human brain. Neuron, 87(1), 231-243.

Tulving, E. (2002). Episodic memory: from mind to brain. Annual review of psychology, 53(1), 1-25.

Tompary, A., & Davachi, L. (2017). Consolidation promotes the emergence of representational overlap in the hippocampus and medial prefrontal cortex. Neuron, 96(1), 228-241.

Vincent, J. L., Kahn, I., Snyder, A. Z., Raichle, M. E., & Buckner, R. L. (2008). Evidence for a frontoparietal control system revealed by intrinsic functional connectivity. Journal of neurophysiology, 100(6), 3328-3342.

Vass LK, Epstein RA (2013) Abstract representations of location and facing direction in the human brain. J Neurosci 33:6133–6142. CrossRef Medline

Woollett, K., & Maguire, E. A. (2011). Acquiring “the Knowledge” of London's layout drives structural brain changes. Current biology, 21(24), 2109-2114.

Winkler, A. M., Ridgway, G. R., Webster, M. A., Smith, S. M., & Nichols, T. E. (2014). Permutation inference for the general linear model. Neuroimage, 92, 381-397.

Wang, C., Chen, X., Lee, H., Deshmukh, S.S., Yoganarasimha, D., Savelli, F., and Knierim, J.J. (2018). Egocentric coding of external items in the lateral entorhinal cortex. Science 362, 945-949.

Woolrich, M. W., Ripley, B. D., Brady, M., & Smith, S. M. (2001). Temporal Autocorrelation in Univariate Linear Modeling of FMRI Data. NeuroImage, 14(6), 1370–1386.

Woolrich, M. W., Behrens, T. E. J., & Smith, S. M. (2004). Constrained linear basis sets for HRF modelling using Variational Bayes. NeuroImage, 21(4), 1748–1761.

Wikenheiser, A. M., & Schoenbaum, G. (2016). Over the river, through the woods: cognitive maps in the hippocampus and orbitofrontal cortex. Nature Reviews Neuroscience, 17(8), 513.

Young, J. J., & Shapiro, M. L. (2011). Dynamic coding of goal-directed paths by orbital prefrontal cortex. Journal of Neuroscience, 31(16), 5989-6000.

Yamada, H., Louie, K., Tymula, A., and Glimcher, P.W. (2018). Free choice shapes normalized value signals in medial orbitofrontal cortex. Nature communications *9*, 162.

Zeithamova, D., de Araujo Sanchez, M. A., & Adke, A. (2017). Trial timing and pattern-information analyses of fMRI data. Neuroimage, 153, 221-231.